An investigation of microstructure and mechanical properties of UV-LIGA nickel thin films electroplated in different electrolytes

2010 J. Micromech. Microeng. 20 025033

(http://iopscience.iop.org/0960-1317/20/2/025033)

J. Micromech. Microeng. **20** (2010) 025033 (9pp) doi:10.1088/0960-1317/20/2/025033

An investigation of microstructure and mechanical properties of UV-LIGA nickel thin films electroplated in different electrolytes

Jun Tang[1], Hong Wang[1,3], XinQiu Guo[2], Rui Liu[1], XuHan Dai[1], Guifu Ding[1] and ChunSheng Yang[1]

[1] Key Laboratory for Thin Film and Microfabrication Technology of Ministry of Education, National Key Laboratory of Micro/Nano Fabrication Technology, Research Institute of Micro/Nano Science and Technology, Shanghai Jiao Tong University, Shanghai 200240, People's Republic of China
[2] Instrumental Analysis Center, Shanghai Jiao Tong University, Shanghai, 200240, People's Republic of China

E-mail: Wanghongsjtu@yahoo.com.cn

Received 2 October 2009, in final form 6 January 2010
Published 29 January 2010
Online at stacks.iop.org/JMM/20/025033

Abstract
Different electrolytes are used to fabricate nickel structures in MEMS devices by the LIGA or UV-LIGA process to meet different requirements. In order to investigate the microstructure and mechanical properties of nickel thin films electroplated in different electrolytes, four sets of nickel specimens were fabricated in different electrolytes: sulfamate bath with both saccharine and butynediol added (type A-I); sulfamate bath with saccharine added (type A-II); watts bath with saccharine added (type B); and chloride bath with saccharine added (type C). The function of these additives was to obtain the stress-free nickel films. The specimens were measured in our uniaxial tensile test system; their surface morphology and fractography, microstructure and texture were studied by SEM, TEM and XRD, respectively. The results show that the four sets of specimens have different mechanical properties and microstructures. The tensile strength of type A-II, type C and type A-I specimens increases with decreasing grain size, which is in accordance with the Hall–Petch law. In contrast, type B specimens have the highest value of ultimate tensile strength and elongation, but with the largest grain size among all the specimens. The XRD results show that there is no preferred orientation in type B while others have a preferred orientation in (2 0 0) along the growth direction. This might be the reason for the difference between type B and other types.

(Some figures in this article are in colour only in the electronic version)

1. Introduction

Electroplated nickel, fabricated by the LIGA or UV-LIGA process, is a promising material for complex structures in micro-electro-mechanical-system (MEMS) devices, such as microprobes, inertial switches [1], micro-nozzles and energy harvest [2], etc. The mechanical properties of the electroplated nickel, which have been studied by many groups, are considered to be critically essential to the MEMS device designing. Sharpe *et al* [3] electrodeposited specimens with 200 μm thickness and 200 μm width and studied them through the uniaxial tensile test. Indentations have been impressed on the surface of the specimen in order to measure the strain by means of interferometric strain/displacement gage (ISDG). Hemker *et al* have also used this technology to study the effect of the post-processing heat treatment on tensile strength [4]. Fritz's group investigated the mechanical properties of

[3] Author to whom any correspondence should be addressed.

Table 1. Compositions of each electrolyte and the electroplating conditions.

Sample	Type A-I sulfamate	Type A-II sulfamate	Type B watts	Type C chloride
$Ni(SO_3NH_2)_2 \cdot 4H_2O$ (g L^{-1})	500	500	0	0
$NiSO_4 \cdot 6H_2O$ (g L^{-1})	0	0	250	0
$NiCl_2 \cdot 6H_2O$ (g L^{-1})	5	5	40	125
H_3BO_3 (g L^{-1})	25	25	35	25
Saccharine (mg L^{-1})	200–300	20–50	50–100	100–150
Butynediol (mg L^{-1})	30–50	0	0	0
pH	4.0	4.0	4.0	4.3
Temperature (°C)	40	45	40	40
Current density (A dm^{-2})	1.0	1.0	1.0	1.0

nickel by using different methods: laser-acoustic method, instrumented microindentation test, as well as resonance frequency measurements [5]. In order to measure the specimen strain, Soboyejo's [6] group impressed two marks on the surface of the specimen by the FIB system. Then the fatigue of LIGA Ni with different thickness was studied. These studies indicate that the mechanical properties of electroplated nickel vary dramatically from that of bulk nickel. Furthermore, their mechanical properties are affected by fabrication conditions, such as temperature, pH and current density [7]. It has also been proved that the additives in the electrolyte contribute to the differences in electroplated nickel's mechanical properties [8] because of their influence on the grain growth. However, the effect of different electrolytes on mechanical properties of electroplated nickel has not yet been systematically studied.

The reason for us to choose three different electrolytes (sulfamate, watts and chloride bath) is that they have unique properties. For instance, the compositions and pH in watts bath remain constant for a long time, but a high electroplating rate cannot be used, due to its limited nickel ion solubility. Compared to watts bath, sulfamate bath can achieve a high electroplating rate, but its compositions are unstable. Although the chloride bath could bring high residual stress in the nickel structure, it has the highest throwing power. The high throwing power ensures a better uniformity of thickness and enables us to electroplate a high-aspect nickel structure. For instance, we have successfully electroplated a 35 μm wide, 350 μm thick nickel structure in chloride bath. But in other baths, we are not able to electroplate the same structure. It is necessary that mechanical properties of the electroplated nickel films in different electrolytes be studied first, and then users could choose a proper electrolyte according to their practical needs.

In this study, four sets of nickel specimens were electroplated in different electrolytes by the UV-LIGA process. Additives were used to obtain stress-free nickel films in practice. Several techniques have been reported to measure the mechanical properties, such as uniaxial tensile test, bulge test, bending test and nanoindentation test, among which the uniaxial tensile test is considered to be the most straightforward and reliable method. A detailed description of this technique was systematically investigated by Sharpe and Hemker [9]. In this paper, the uniaxial tensile tests were carried out to measure the mechanical properties of the specimens in our system [10]. Then, the scanning electron microscope (SEM) images were used to observe the surface morphology and fractography of different specimens. Their microstructures were directly characterized by transmission electron microscopy (TEM), and their texture was studied by x-ray diffraction (XRD). The differences in their mechanical properties, microstructure and texture were discussed.

2. Experimental and measuring procedure

2.1. Tensile test specimen fabrication

Table 1 lists the compositions of four different electrolytes and the electroplating conditions. In order to obtain stress-free structures, additives such as saccharine and butynediol are used to offset the residual stress by inducing compressive or tensile stress. The saccharine additive was added into the sulfamate (type A-I), watts (type B) and chloride baths (type C) until stress-free nickel structure was obtained. Meanwhile, both saccharine and butynediol were added into the sulfamate bath (type A-II) in order to study the effect of different additives on mechanical properties. A magnetic pellet was used to stir the solution to prevent the generation of hydrogen bubbles on the specimen surface.

The test chips were designed and fabricated on the glass substrate by the UV-LIGA process, shown in figures 1(*a*)–(*i*). The fabrication process flow was drawn from the cross-section view of the specimen in figure 1(*j*). First, the free-standing specimens were electroplated on the positive photoresist sacrificial (PR) layer, and two displacement marks were impressed on the specimen with a distance about 100 μm by using the hardness tester, figures 1(*a*)–(*d*). These two indentations are square with sides of 5 μm, and the penetrated depth is about 0.7 μm. These marks enable us to measure the strain through the CCD images. A similar indentation method was also used in Sharpe's [3] and Soboyejo's studies [6]. Then, the 40 μm thick supporting frame and springs were electroplated to align the specimen along the tensile direction, and to protect the specimen from damage during the assembling process, figures 1(*e*), (*f*). After that, the test chip was stripped from the glass substrate by removing the sacrificial layer in 3%wt NaOH solution at room temperature, figures 1(*g*), (*h*). Finally, the seed layer was removed in the ammonia/peroxide solution figure 1(*j*). During the fabrication process, the thickness of the specimen was monitored by stylus profiler (Dektak 6M, Veeco, USA), by

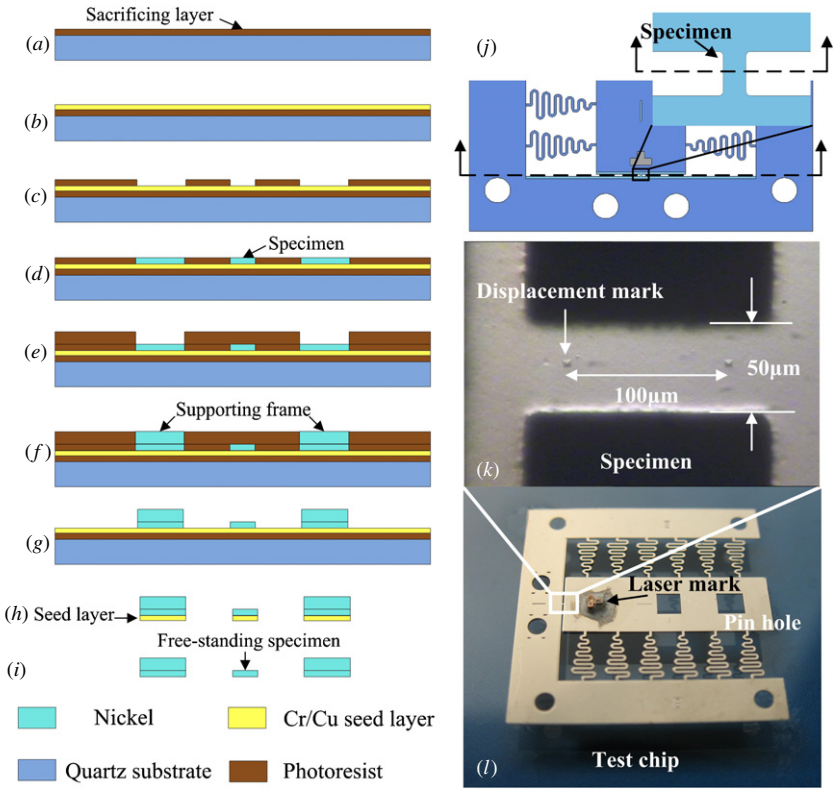

Figure 1. Fabrication process of specimen (*a*)–(*i*), cross-section view of the specimen (*j*), optical images of the specimen (*k*) and the test chip (*l*).

controlling electrodepositing time and current density. The gauge of the specimen is 50 μm wide, 150 μm long and 10 μm thick. The optical images of the test chip and the specimen are shown in figures 1(*k*), (*l*). The design and fabrication details of the tensile test specimen are given in [11, 12].

2.2. Tensile test procedure

The uniaxial tensile test system, as shown in figure 2, mainly consists of a force sensor, a laser displacement sensor, a piezoelectric step motor, a vacuum-absorb table, a microscope and a computer controller. First, the test chip was fixed in the vacuum-absorb table; then, the force sensor was connected to the test chip through two pin-holes; the laser displacement sensor was adjusted to focus on the laser mark on the test chip to record the strain of the specimen and to monitor the tensile process; after that, the force was applied by the piezoelectric step motor which was controlled by the computer. The tensile force is calculated as $F = k_f\delta$, where k_f is the spring constant of the force sensor, which was accurately calibrated before the test; δ is the deformation of the force sensor. Simultaneously, the *in situ* images of the specimen, which are necessary for the postprocessing strain calculation, were recorded by the CCD camera which was fixed on the microscope; the displacement sensor also recorded the strain of the specimen at the same time, informing the tensile status in real time; finally, after the fracture of the specimen, another tensile process was carried out to determine the sum of the spring constant of the 12 supporting springs k_s. As a result, the stress can be calculated as $s = \frac{(k_f - k_s)\delta}{wt}$, where w is the width and t is the thickness of the specimen. The strain was calculated from CCD images and the laser-displacement sensor. The resolution of the laser-displacement sensor is 10 nm, which ensures the accuracy of strain measurement during the test. The computer controlled the entire tensile process and recorded the data. The detailed description of the tensile system and the procedure are given in [10, 11].

2.3. SEM, XRD and TEM tests

The SEM images were acquired by Zeiss SEM ultra 55 to study the surface morphology and the fractography of different nickel specimens. The SEM sample platform was set to 55° inclined to the horizontal plane during the observation of the cross section of the fractured specimens. The x-ray diffraction (XRD) test was carried out (Rigaku D/max-2550, Japanese) to study the texture of the four types of nickel thin films. The specimens with 20 μm thickness were electroplated under the same conditions corresponding to the four sets of tensile specimens and were tested using the micro-hardness tester (HXD-1000TMB/LCD, China). The microstructures of the four sets of the nickel specimens were directly characterized by TEM bright-field images and the diffraction patterns by using a TEM (JEM-2010/JEOL Japanese) at Instrumental Analysis Center of Shanghai Jiao Tong University. Since it is difficult to fabricate TEM samples, an efficient method was developed by

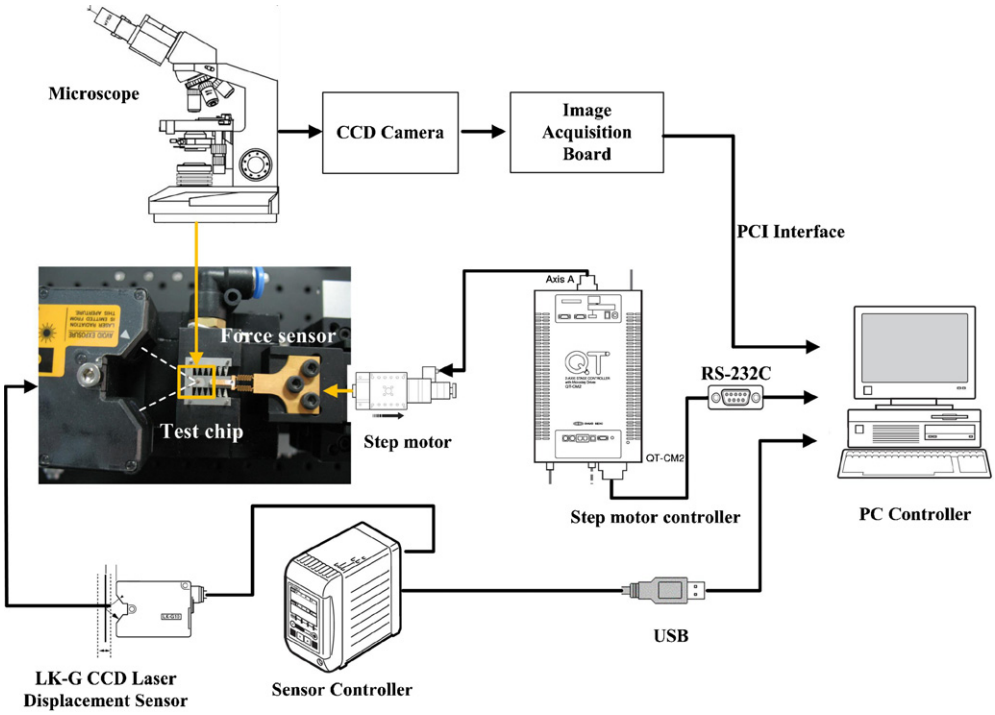

Figure 2. Schematic of the uniaxial tensile test system.

using the UV-LIGA process in this study. First, a 10 μm thick positive photoresist (PR) was spun on the glass substrate as the sacrificial layer, and then a Cr/Cu seed layer was sputtered on it; the third 15 μm thick PR layer was spun on the top and patterned to 3 mm diameter holes; after that, the TEM samples were electroplated; finally, the TEM samples were stripped off by removing the underlying sacrificial layer. The TEM sample with 10 μm thickness and 3 mm diameter was ion polished by the Gatan model 691 precision ion polishing system until a hole appeared at its center, which signified the accomplishment of the specimen preparation. Then both the TEM bright-field and dark-field images were used to calculate the grain size of the nickel specimens.

3. Results and discussion

3.1. Surface morphology

Figure 3 shows the SEM images of the surfaces of the nickel specimens electroplated in different electrolytes. When only saccharine is added to sulfamate (type A-II), watts (type B) and chloride baths (type C), type B specimens have the smoothest surface (figure 3(*c*)); type A-II specimens have the roughest surface (figure 3(*b*)); type C specimens are in between (figure 3(*d*)). The surfaces of type A-I and type A-II specimens electroplated in sulfamate bath, but with different addtitives, are also quite different. Type A-I specimens (figure 3(*a*)) have a very smooth surface compared to that of type A-II (figure 3(*b*)). It indicates that the electrolyte with both saccharine and butynediol additives can produce a Ni structure with finer grain and smoother surface.

3.2. Tensile test result

8–12 specimens of each set were tested in our tensile test system. The results show that the fracture mechanism and the value of ultimate tensile strength and elongation in each set are in good agreement. The engineering stress–strain curves of different specimens are shown in figure 4. When the gauge length is 100 μm, the average elongations of type A-I, type A-II, type B and type C specimens are 7.94%, 12.38%, 13.90% and 10.22%, respectively. Considering the condition that sulfamate, watts and chloride baths have added saccharine to obtain stress-free nickel thin film, all the specimens show high elongation, which suggests their good ductility. Type B specimens have the highest ultimate strength; type A-II specimens have the lowest ultimate tensile strength; the ultimate tensile strength of type C specimens is in between. The ultimate strength of type A-I specimens is much higher than that of type A-II, which indicates that the electroplated nickel thin film in sulfamate bath is strengthened by adding both saccharine and butynediol. This is because two additives in the electrolyte have more effect on the crystallization during the electroplating process, which leads to a finer grain nickel structure; and the finer grain structure increases the strength of metal materials.

The average ultimate tensile strength and the hardness of type A-I, type A-II, type B and type C specimens are 1954 MPa and 4.47GPa, 923 MPa and 2.87GPa, 2178 MPa and 4.64GPa, 1525 MPa and 4.31GPa, respectively, which are significantly larger than that of bulk nickel (483 MPa for ultimate strength) and many other reports [3, 13, 14]. Many groups have reported that such ultra-high strength can be obtained in nano-grained nickel structures [15–17]. When the

Table 2. The mechanical properties of the four types of nickel specimens and comparisons between recent similar studies.

Studies	Electroplating solution	UT strength (MPa)	Elongation (%)	Hardness (GPa)	Mean grain size	Current density (mA cm^{-2})
Current study	Type A-I	1954	7.94	4.47	∼20 nm	10
Current study	Type A-II	923	12.38	2.87	∼160 nm	10
Current study	Type B	2178	13.90	4.64	∼420 nm	10
Current study	Type C	1525	10.22	4.31	∼55 nm	10
Sharpe	Unknown	555	–	–	–	–
Yang [15]	Sulf	1952	–	–	15 ± 5 nm	50
Dalla Torre [16]	Purchased	2040	–	6.0	20 ± 3 nm,	–
	Purchased	1820		5.5	21 ± 4 nm	–
Stephens [17]	Watts	2100	–	3.92	<1 μm	30
	Sulf	1600		3.92	<1 μm	30

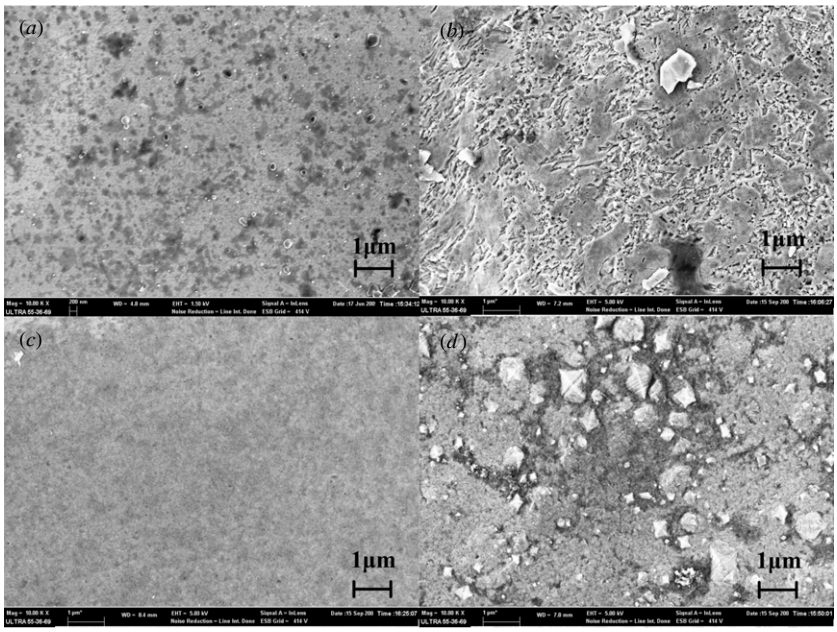

Figure 3. SEM images of the electroplated nickel surface of type A-I (*a*), type A-II (*b*), type B (*c*) and type C (*d*).

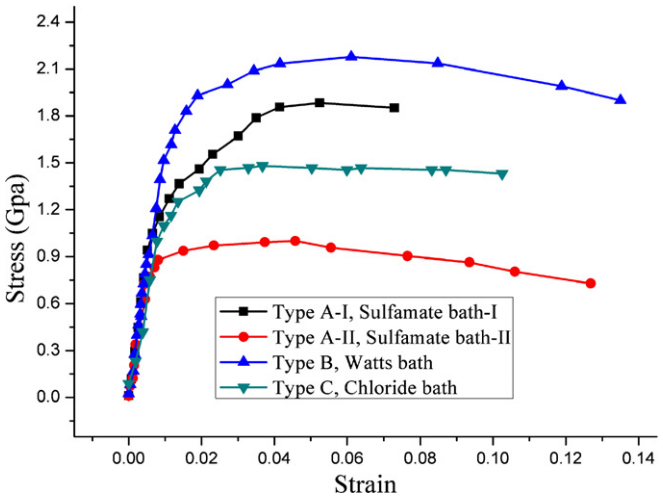

Figure 4. The engineering stress–strain curve of four types of specimens.

grain size of the specimens is about 20 nm, the ultimate tensile strengths measured in Yang's work [15] and Dalla Torre's work [16] are 1952 MPa and 2040 MPa, respectively. These measured mechanical properties of nickel together with our results were listed in table 2 for comparison. Table 2 also lists the grain size of the specimens. The detailed description of the microstructure of our specimens will be discussed in section 3.3. Since the electroplating conditions, specimen size and the measurement vary in different studies, the discrepancy in the values listed in table 2 is reasonable. For instance, the ultimate tensile strength of nickel measured by Sharpe's group is 555 MPa [3], which is much smaller than other results. The gauge of our specimens was 50 μm wide and 5 μm thick, which is much smaller than the specimen used in Sharpe's work (200 μm wide and 200 μm thick). It has been demonstrated that smaller size of the specimen would lead to higher strength [15, 18]. Moreover, the grain size of the specimens in this paper is very small since the additives were used in the electrolyte, which also contributes to an ultra-high tensile strength compared to Sharpe's work.

All the data listed in table 2 are obtained from dog-bone tensile specimens except Stephens' [17], which is obtained from microposts by the bending approach. This leads to the discrepancy between the test results. However, Stephens's

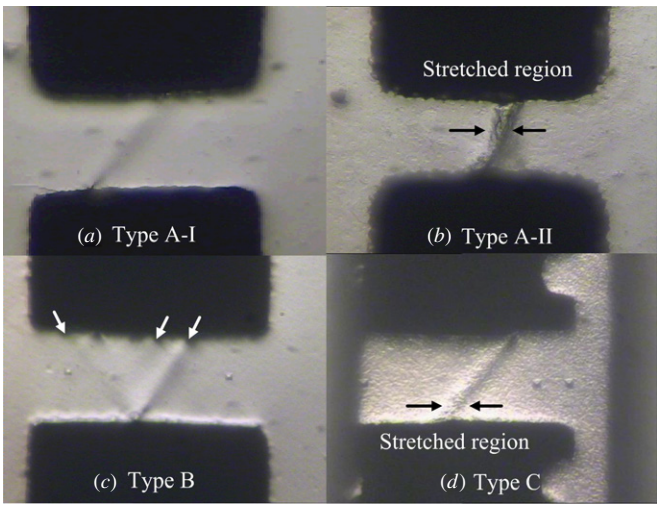

Figure 5. Top-view optical images of different specimens before the rupture.

work [18] suggests that the tensile strength of Watts nickel is much higher than that of sulfmate nickel, which is also observed in our study. Watts nickel (type B) specimens have the highest tensile strength while their grain size is the largest among the four sets of specimens. Moreover, the other three sets of nickel are in accordance with the Hall–Petch law. Their strength increases with decreasing grain size and elongation. The XRD test was carried out to find the reason why type B disobeys the Hall–Petch law. It will be discussed it in section 3.4.

The applied displacement speed of all four sets of specimens was set to 0.2 μm s^{-1}, but the strain rate in the test turned out to be much smaller. The average strain rates of type A-I, type A-II, type B and type C specimens are 1.8×10^{-4} s^{-1}, 1.84×10^{-4} s^{-1}, 0.945×10^{-4} s^{-1}, 1.55×10^{-4} s^{-1}, respectively. There is only slight difference in the strain rate among the four sets of the specimens. This difference lies in specimens' different mechanical properties. Dalla Torre *et al* have studied the influence of the strain rate in the tensile test on mechanical properties of electroplated nickel [19]. They have proved that when the strain rate is below 10^0 s^{-1}, the ultimate tensile strength remains constant, while the elongation changes. But only a large decrease in the strain rate can bring a little increase in the elongation. Thus, the slight strain rate difference does not affect the mechanical properties among the four sets of specimens.

The *in situ* top-view images of the specimens were captured during the tensile process. Shear fracture was observed in type A-I, type B and type C specimens. The cracks initiated at the specimen's edge. Differently, the type A-II specimen eventually produced a necked region. Both the shear fracture and the necked region are typical forms of ductile fracture, which accords with the ductility of electroplated nickel observed in the tensile tests. Furthermore, before the type B specimens rupture, several cracks on the active slip plane have occurred at approximately 55° to the tensile axis, shown by arrows in figure 5(*c*). The same phenomenon has also been found in Dalla Toorre's study [16]. The fracture of type A-I is similar to that of type B. Their crack is very narrow; they both have a very smooth surface shown in figures 5(*a*), (*c*). It has also been observed in the SEM images, figures 3(*a*), (*c*). The similarity of the fracture between type B and type A-I may be related to their ultra-high tensile strength and hardness. Although the fracture of type C specimens is also shear fracture, the crack has a stretched region, which might be related to its higher ductility, lower ultimate tensile strength and hardness (figure 5(*d*)). The top view of type A-II specimen before it ruptures is significantly different from that of other types of specimens. A necked and stretched region occurred, and the crack is no longer inclined at a certain angle to the tensile axis. The wide-stretched region might be related to its highest ductility and lowest strength.

3.3. Fractography

The SEM images of the cross section of type A-I, type A-II, type B and type C specimens were used to analyze the fractography, shown in figures 6(*a*, *c*), (*b*, *d*), (*e*, *h*) and (*f*, *h*) respectively. Type A-I, type B and type C all show ductile dimple ruptures in their fracture cross sections. Specifically, type A-I has both dimple and cleavage fracture. The cleavage fracture is a flat facet occurred along the slip plane; this cleavage fracture might be brought about by its lowest ductility and elongation. The dimple rupture, with a diameter of about 100–200 nm microvoids, occurs at the edge of the specimen, marked by arrows in figure 6(*c*). Both fractures of type B and type C are characterized by dimple rupture, which suggests that they are more ductile than type A-I. It is coherent with their higher elongations in the tensile test. The size of microvoids in the fractures of type B and type C are about 100 nm and more than 200 nm, respectively, shown in figures 6(*e*), (*f*). The fracture of type C specimen has a stretched region, which is also observed in the top-view images before the fracture (figure 5(*d*)). Among the four sets of different specimens, the fractography of type A-II specimen shows a necked region. Its crack is almost perpendicular to the tensile direction while others have cracks inclined at a certain degree to the tensile direction. Dimple rupture can be observed in some areas of the cross section. The different fractography of type A-II might be related to its lowest ultimate tensile strength and hardness, and its high ductility.

3.4. Microstructure and texture

Figure 7 shows the TEM bright-field images together with the corresponding SAD patterns of type A-I (*a*), type A-II (*b*), type B (*c*) and type C (*d*). The grain sizes of the specimens are calculated from both bright-field images and dark-field images in the selected areas. The results show that the type A-I nickel film has the mean grain size of about 20 nm with a narrow distribution; the mean grain sizes of type A-II, type B and type C are about 160 nm, 420 nm and 55 nm, respectively, but with a wide distribution. The mean grain sizes of different types of specimens are listed in table 2. Meanwhile, all the selected area diffraction patterns (SADP) are ring diffraction patterns, showing that the electroplated nickel is polycrystalline material. The specimen with a larger

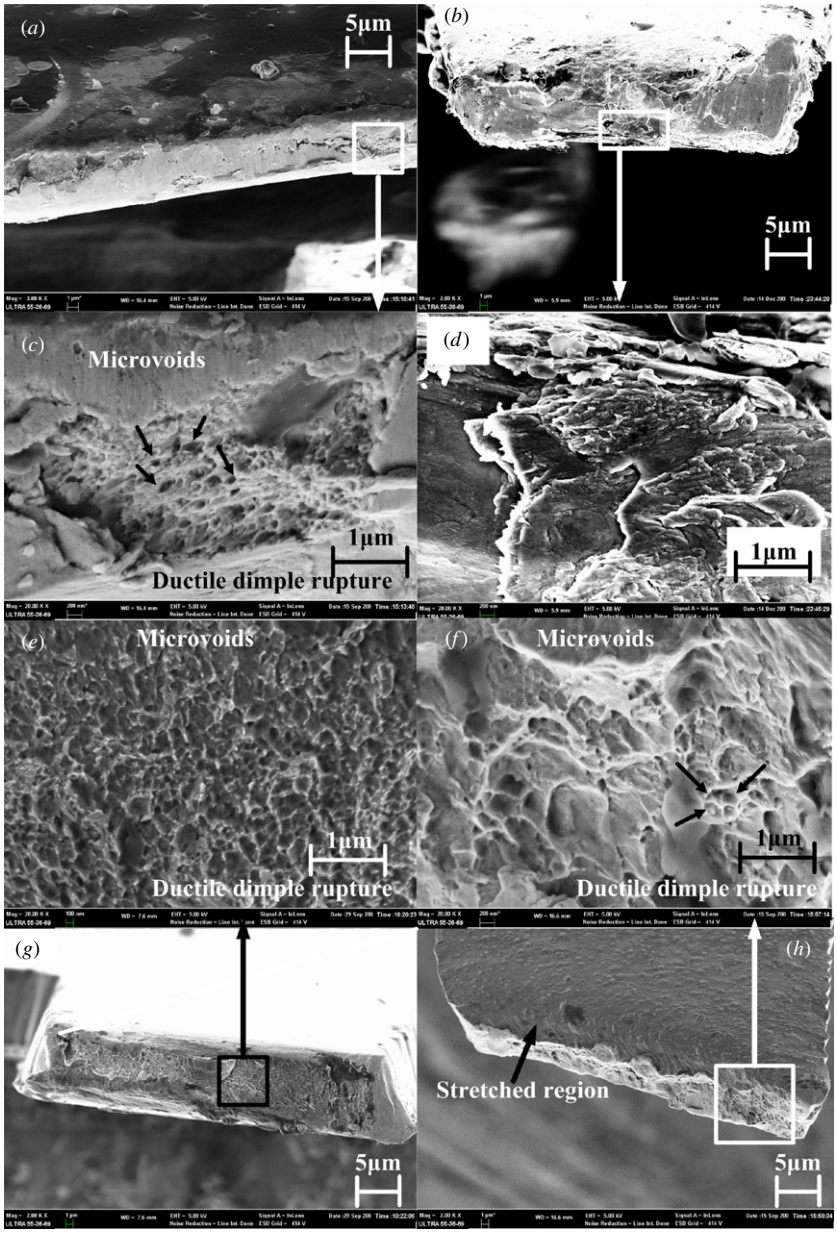

Figure 6. Fractography of type A-I (*a*), (*c*), type A-II (*b*), (*d*), type B (*e*), (*g*) and type C (*f*), (*h*) specimens.

grain size has a more speckled ring pattern made up of discrete spots, shown in figure 7.

The XRD result of the different electroplated nickel specimens is shown in figure 8. Compared to the standard Ni sample with a fully random crystal orientation, beside type B, all other three sets of nickel specimens have a preferred orientation in (2 0 0) direction perpendicular to the surface, but with different degrees. Among these three sets of electroplated nickel, type A-II has the strongest preferred orientation in (2 0 0) direction. Type C also has a very strong (2 0 0) orientation, whereas type A-I shows a much weaker orientation than the former two types. Interestingly, type A-I, type A-II and type C obey the Hall–Petch law. Their tensile strength increases with the decrease of their grain sizes. In contrast, type B nickel specimens have a fully random crystal orientation. This might explain why type B nickel does not obey the Hall–Petch law. As we can see, type B specimen has the highest UT strength but with the largest grain size. It reveals that anisotropy exists in the electroplated nickel film. Stephens *et al* also found that the nickel structure electroplated in watts bath has a much higher UT strength than that electroplated in sulfamate bath [17]. It is because nickel electroplated in watts has a uniform randomly oriented grain structure, which is different from the columnar grain structure along the growth direction in the nickel specimen electroplated in sulfamate bath. As a result, the type B watts specimens have the highest UT strength and longest elongation. Thus, it is necessary to study the watts bath in the electroplating process in the future.

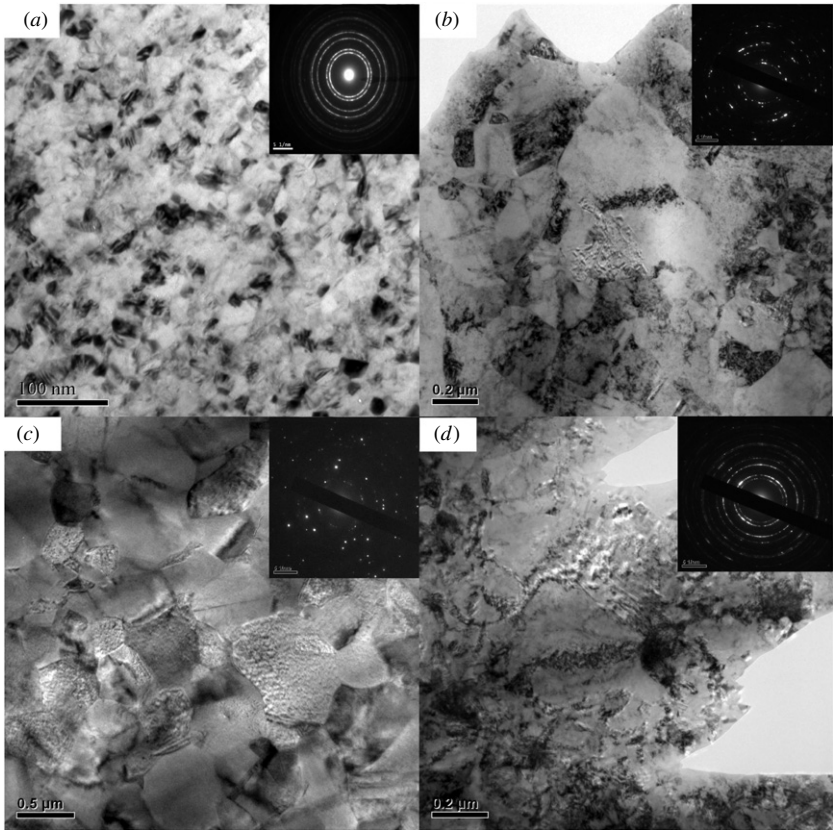

Figure 7. TEM bright field images together with the corresponding SAD patterns of type A-I (*a*), type A-II (*b*), type B (*c*) and type C (*d*).

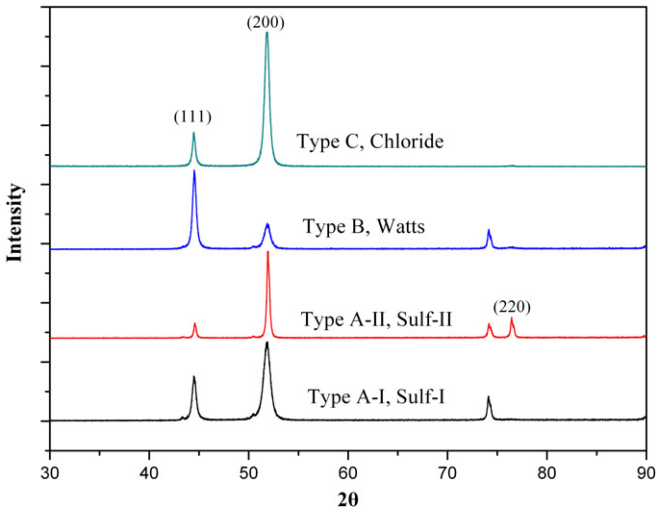

Figure 8. X-ray diffraction spectra of nickel specimens electroplated in different electrolytes.

4. Conclusions

The four sets of different nickel specimens were electroplated in sulfamate bath with both saccharine and butynediol added (type A-I), sulfamate bath with saccharine only added (type A-II), watts bath with saccharine added (type B), chloride bath with saccharine added (type C), respectively. The additives were added to obtain stress-free nickel film. The surface morphology and fractography, microstructure and texture were studied by SEM, TEM, XRD, respectively. The values of tensile strength, hardness and elongation were obtained under a certain conditions in our experiment and the results show the distinctions in the different electroplated nickel films.

(1) The average ultimate tensile strength and hardness of type A-I, type A-II, type B and type C specimens are 1954 MPa and 4.47GPa, 923 Mpa and 2.87GPa, 2178 MPa and 4.64GPa, 1525 MPa and 4.31GPa, respectively; when the gauge length is 100 μm, the average elongations of type A-I, type A-II, type B and type C specimens are 7.94%, 12.38%, 13.90% and 10.22%, respectively. The mechanical properties suggest that all the specimens have high ductility and high ultimate tensile strength compared to that of bulk nickel. Type A-II specimen shows a knife-edge rupture while others have a ductile dimple rupture.

(2) The surfaces of type A-I and type B specimens are very smooth, whereas those of type A-II and type C are rough. The mean grain sizes of type A-I, type A-II, type B and type C specimens are about 20 nm, 160 nm, 420 nm and 55 nm, respectively. Except for type B (watts bath), the tensile strength of the other three sets increase when their grain sizes decrease and they all show good agreement with the Hall–Petch law.

(3) The XRD results suggest that type B nickel specimens have a fully random crystal orientation while the other three sets of electroplated nickel show a preferred orientation in the (2 0 0) direction along the growth

direction. This might explain why the watts bath-electroplated nickel specimen does not obey the Hall–Petch law. This also demonstrates that anisotropy exists in electroplated nickel.

Acknowledgments

This research is supported by the National Hi-Tech Research and Development Program of China under grant (2006AA04Z360), the Cultivating Foundation for Innovation Engineering Program of the Ministry of Education of China under grant (708037) and the National Key Laboratory Foundation (9140C79030302090C79).

References

[1] Yang Z, Ding G, Cai H, Xu X, Wang H and Zhao X 2009 Analysis and elimination of the 'skip contact' phenomenon in an inertial micro-switch for prolonging its contact time *J. Micromech. Microeng.* **19** 045017–27

[2] Wang P, Tanaka K, Sugiyama S, Dai X, Zhao X and Liu J 2009 A micro electromagnetic low level vibration energy harvester based on MEMS technology *Microsyst. Technol.* **15** 941–51

[3] Sharpe W N, LaVan D A and Edwards R L 1997 Mechanical properties of LIGA-deposited nickel for MEMS transducers *1997 Int. Conf. on Solid-state Sensors and Actuators (Chicago, 16–19 June 1997)* pp 607–10

[4] Hemker K J and Last H 2001 Microsample tensile testing of LIGA nickel for MEMS applications *Mater. Sci. Eng.* A 882–6

[5] Fritz T, Griepentrog M, Mokwa W and Schnakenberg U 2003 Determination of Young's modulus of electroplated nickel *Electrochim. Acta.* **48** 3029–35

[6] Allameh S M, Loua J, Kavishe F, Buchheit T and Soboyejo W O 2004 An investigation of fatigue in LIGA Ni MEMS thin films *Mater. Sci. Eng.* A **371** 256–66

[7] Luo J K, Pritschow M, Flewitt A J, Spearing S M, Fleck N A and Milne W I 2006 Effects of process conditions on properties of electroplated Ni thin films for microsystem applications *J. Electrochem. Soc.* **153** D155–61

[8] Lim J H, Park E C, Joo J and Jung S-B 2009 Effect of additives on microstructure and mechanical properties of nickel plate/mask fabricated by electroforming process *J. Electrochem. Soc.* **156** D108–12

[9] Hemker K J and Sharpe W N Jr. 2007 Microscale characterization of mechanical properties *Ann. Rev. Mater. Res.* **37** 93–126

[10] Liu R, Li X P, Wang H and Ding G 2008 A micro-tensile method for measuring mechanical properties of MEMS materials *J. Micromech. Microeng.* **18** 065002–9

[11] Tang J, Wang H, Li S C, Liu R, Mao S P, Li X P, Zhang C C and Ding G 2009 Design and fabrication of micron scale free-standing specimen for uniaxial micro-tensile tests *J. Micromech. Microeng.* **19** 105015–24

[12] Liu R, Li X P, Wang H and Ding G F 2008 Analysis, simulation and fabrication of MEMS springs for a micro-tensile system *J. Micromech. Microeng.* **19** 015027–37

[13] Cho H S, Hemker K J, Lian K, Gottert J and Dirras G 2003 Measured mechanical properties of LIGA Ni structures *Sensors Actuators* A **103** 59–60

[14] Mazza E, Abel S and Dual J 1996 Experimental determination of mechanical properties of Ni and Ni-Fe microbars *Microsyst. Technol.* **2** 197–202

[15] Yang Y, Imasogie B I, Allameh S M, Boyceb B, Lian K, Loua J and Soboyejo W O 2007 Mechanisms of fatigue in LIGA Ni MEMS thin films *Mater. Sci. Eng.* A **444** 39–50

[16] Dalla Torre F, Spätig P, Schäublin R and Victoria M 2005 Deformation behaviour and microstructure of nanocrystalline electrodeposited and high pressure torsioned nickel *Acta Mater.* **53** 2337–49

[17] Stephens L S, Kelly K W, Simhadri S, McCandless A B and Meletis E I 2001 Mechanical property evaluation and failure analysis of cantilevered LIGA nickel microposts *J. Microelectromech. Syst.* **10** 347–59

[18] Son D, Kim J, Kim J-Y and Kwon D 2005 Tensile properties and fatigue crack growth in LIGA nickel MEMS structures *Mater. Sci. Eng.* A **406** 274–8

[19] Dalla Torre F, Van Swygenhoven H and Victoria M 2002 Nanocrystalline electrodeposited Ni: microstructure and tensile properties *Acta Mater.* **50** 3957–70